

# Surface Topography as an Energy State: Hamiltonian Description of Functional Properties in Phase Space and Quantification via Optical Methods

Boris Brodmann<sup>1</sup>, Matthias Eifler<sup>2</sup>

<sup>1</sup> OptoSurf GmbH, Ettlingen, Germany

<sup>2</sup> IU International University of Applied Sciences, Erfurt, Germany

## Abstract

The assessment of tribological processes necessitates comprehensive monitoring and interpretation of surface states, traditionally by topography height values and surface texture parameters. This paper proposes a phase space representation as generic interpretation of surfaces to enhance tribological assessments. By deriving distinctions between two-dimensional and three-dimensional manifolds from phenomenological thermodynamics, we demonstrate the existence of fractal dimensions on physical surfaces. Utilizing the smallest representable wavelength, a coordinate ensemble where each coordinate has a generalized degree of freedom and a differential amount across fractal dimensions is proposed. The metric is interpreted as a time coordinate, allowing the derivative to be seen as velocity. Through geometric dimension analysis, we derive a topographic Hamiltonian via generalized momentum. Each coordinate pair in the ensemble is assigned a location in phase space. Statistical considerations define a symplectic structure and phase space volume. As a use-case, a two-disc experiment demonstrates that topography changes under load can be understood as a self-organization process through thermodynamic reasoning. As a possibility for a direct assessment of the phase space of a surface for monitoring tribological processes, we propose the combination of topographic measuring systems with scattering light measurement. This multi sensor approach offers opportunities for optimizing performance in tribological applications.

## 1. Motivation

Surfaces present unique challenges across various research disciplines. Wolfgang Pauli aptly captured this when he remarked, "God created volume, but the devil created the surface." This quote highlights the complex nature of interfaces between objects. A fascinating example is Evangelista Torricelli's Gabriel's Horn, which demonstrates that a body with finite volume can possess an infinitely large surface area [1]. Similarly, Jacob Beckenstein made a fundamental contribution by showing in his thermodynamic analysis of black holes that the information about objects falling beyond the event horizon is encoded in the surface area, not the volume [2].

This special significance of surfaces is also reflected in tribology, where their properties play a central role. Surfaces separate the volumes of base and counter bodies as well as the intermediate and surrounding media. Under a collective of stresses—comprising mechanical, thermal, chemical, and physical influences such as radiation or electric fields—their properties change over time. These changes can be quantified through dissipative processes in the form of material and performance losses, which in turn lead to different forms of wear [3]. The processes driving these changes are diverse and interconnected. Their mechanisms can be explained on the respective scales, but their overall effect can only be understood in interplay. Especially in tribology, it becomes clear that surfaces are not just static interfaces but dynamically changing entities that significantly influence the function and efficiency of a system.

A central goal of tribology is to avoid direct contact between friction partners by using an appropriate separating lubricant film and to protect the base body by selectively altering the chemical potential in the boundary layer volume. These dynamic processes require a variety of interdisciplinary approaches, ranging from hydrodynamics, continuum mechanics, chemistry, materials science, to the study of machine elements. The geometric properties of the surface are also usually considered in tribological

considerations in the form of roughness. In the plasticity index for the contact of rough surfaces developed by Greenwood and Williamson, there is a purely geometric term consisting of the quotient of the average asperity height and their average radius of curvature. This index allows predicting the elastic or plastic behavior of surface contacts, which is essential for the design and optimization of tribological systems [4]. On a very elementary level, it connects the material properties of the boundary layer volume and their geometric interface. This model has been further developed by many works, including Nayak [5], who uses the statistical moments of the spectral power density to characterize roughness and introduces the contact mechanical parameter  $\alpha$ , which consists of the central moments of the Power Spectral Density (PSD). Whitehouse/Archard, however, emphasize the dependence of the PSD on random influences during its metrological quantification and alternatively propose using the autocorrelation length of a surface profile section to calculate an average asperity width [6]. Persson, however, shows in [7] the outstanding importance of the properties of the PSD for the mechanical contact of rough surfaces and integrates the fractal dimensions introduced by Mandelbrot into a more general model. Central to this is the Hurst exponent  $H$ , which corresponds to the slope of the PSD in the logarithmic representation and can be described by the relationship  $D = E - H$ , where  $D$  is the fractal dimension and  $E$  is the embedded dimension, i.e., the one in which the body exists. For rough surfaces, this approach has already been proposed by Gagnepain and Roques-Carnes as a method for characterization [8].

However, Whitehouse rejects the practical significance of the spectral power density and the Hurst exponent for characterizing a topography. He emphasizes that fractal dimensions cannot have practical relevance for metrological quantification due to their sensitivity to high-frequency components, which are strongly influenced by non-systematic measurement deviations [9]. Typical sources of error such as noise, limited measurement resolution, or calibration uncertainties lead to distortions, particularly in the high-frequency regions of the PSD, and affect the calculation of fractal parameters like the Hurst exponent. Instead, Whitehouse advocates more robust approaches such as the autocorrelation function, which is less susceptible to noise and allows direct conclusions about the average structure of the surface. The average gradient  $\Delta q$  of the microstructure is particularly affected, as its value predominantly depends on high spatial frequencies that is shown in the appendix of [10]. Although Mayers [11] has already demonstrated a strong correlation of  $\Delta q$  with friction properties and its significant tribological importance has been theoretically presented by Molinari et al. and Popov [12][13], it has not yet gained significant relevance in application due to the metrological uncertainties frequently mentioned by Whitehouse, e.g., in [14]. Nevertheless, initial approaches for various applications have been established. For example,  $Rdq$  is recommended for describing the surface of ball pivots [15], and gear elements, such as the flank roughness of worm gears, show a high correlation of the gearbox efficiency with the average profile angles [16].

Tevis et al. [17] clearly emphasize the position of the PSD as a topographical feature, suggesting that the topography itself should be considered a material property, thus highlighting the original challenge that the surface holds a special position as a subset of a volume that can come into tribological contact with another body.

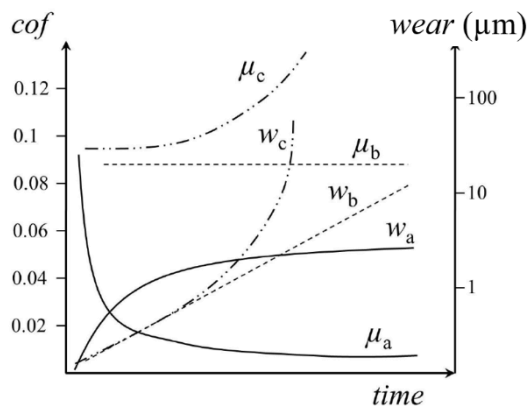


Fig. 1a) Different wear and friction behavior of tribological systems [16]

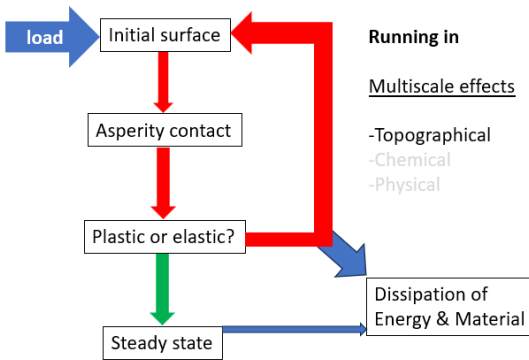


Fig. 1b) Process of topographical running in and the “exit” point with the steady state regime

Since tribology considers changes in a system regarding the dissipation of work and material over time, it obviously deals with thermodynamic systems that are not in equilibrium [18]. Due to the continuous input of mechanical work, the interaction of system components with the collective of stresses is enabled. Friction and wear lead to dynamic system behavior and result in performance and material losses. In a review publication [19], Scherge shows three possible process sequences, which are illustrated in Figure 1a as a schematic representation of how the system behavior can evolve from the initial state with regard to wear rate  $w$  and friction coefficient  $\mu$ . The three scenarios are the catastrophic scenario (c), a constant course (b), or a favorable so-called system run-in (a), where the friction coefficient decreases and, along with the wear rate, asymptotically approaches a stable operating state. When viewed in a system diagram, as shown in Figure 1b, the surface in contact is continuously confronted with the question of whether the deformations in the load-bearing contact areas are elastic or plastic. Plastic deformation carries the potential for material loss due to shear forces, and the deformation work expended leads to dissipation of mechanical power. In a favorable course of events, the tribological system utilizes the frictional work to shift from the plastic to the elastic regime. The shearing and plastic deformation of non-load-bearing asperities changes the geometric conditions, so that the necessary deformation work becomes reversible, and molecular interactions between the friction partners can stabilize at a low level. If the mechanism already suspected by Archard [20] is applied, which states that asperities plastically deform under load until they reach a purely elastic state, then the process sequence for tribological processes shown in Figure 1b results.

A generally accepted process assumes the formation of a “third body” under favorable running-in conditions [21], which can be understood as part of self-organized structure formation. Nosonovsky describes this aspect of non-equilibrium thermodynamics in his article "Entropy in Tribology" [22]. He attributes information content to the microgeometry of roughness and interprets the change in the height distribution (ADF) during the running-in phase as entropy reduction and thus as a process of self-organization. However, his entropy approach negates that Shannon entropy describes the diversity of possible arrangements in a distribution, i.e., the number of possible microstates of an ensemble. Carcassi points out that a symplectic structure of the system components is necessary for this [23], which must be described in phase space.

Brodmann outlines a possibility for this in [24] by interpreting the density distributions of ordinates and gradients described by Peklenik [25] as statistical degrees of freedom of spatial and momentum information and demonstrates that a randomly rough surface can be understood as a microstate of a statistical ensemble. Since the additional use of the gradient for the necessary topography description

enables the calculation of a surface area, an analogy to the concept of entropy of a surface introduced by Bekenstein is also offered. He uses entropy  $S$  as a measure of the information for the matter that has passed into the black hole:

$$S = A \frac{4k_B}{l_p^2}$$

( $k_B$ : Boltzmann constant;  $l_p$ : Planck length;  $A$ : surface area of the event horizon)

In the following, it will be shown that physical bodies consisting of condensed matter must necessarily have a fractal surface and that this surface possesses a symplectic structure on every chosen scale.

## 2. Derivation of the existence of fractal surfaces from the state variables of phenomenological thermodynamics

The starting point of the description is the consideration of a gaseous medium and the ideal gas law ( $PV = CT$ ), which describes the behavior of an ideal gas in limiting cases. This relation can be established for both an atomistic and a continuous medium, but it cannot describe phase transitions and thus no interfaces. However, the real behavior of a medium during temperature, pressure, or volume changes does, of course, include phase transitions. Only by introducing the van der Waals equation for real gases

$$P(V) = \frac{nRT}{V - b} - \frac{n^2a}{V^2},$$

which considers the intermolecular interactions and the finite volume of the particles, a phase transition can occur. It extends the ideal gas law by including the space occupied by gas molecules  $b$  and the so-called cohesion pressure  $a$ , which defines the intermolecular forces.  $P(V)$  is the volume-dependent function of pressure  $P$  at a given temperature  $T$ ,  $R$  is the ideal gas constant (the product of Avogadro's number  $N_A$  and the Boltzmann constant  $k_B$ ) and  $n$  is the number of particles involved. Below a critical temperature and certain pressure-volume ratios, the kinetic energy of some particles in the ensemble can no longer overcome the attractive forces of the cohesion pressure  $a$  so that a change in volume does not lead to any further change in pressure, as these particles are no longer part of the gas volume but of the formed body. The energy of this body will thus be composed of the remaining kinetic energy of the particles that make it up, the binding energy between them, and the pressure exerted on its volume from the outside. In thermal equilibrium, this will be determined by the most probable particle velocity distribution (temperature  $T$  and entropy  $S$ ), the number of particle bindings (chemical potential  $\mu$  and the number of particles involved  $N$ ), as well as the pressure  $P$  acting on the body's volume  $V$  from the outside.

Considering the internal energy  $U = TS - PV + \mu N$ , it can be divided into a kinetic component, determined by the Maxwell-Boltzmann distribution described by the Temperature  $T$  and Entropy  $S$ , a potential component, given by the volume work term  $PV$ , and the chemical potential  $\mu$ . In a potential-free environment, where only the interactions between the particles exist, the kinetic energy of some particles will no longer be sufficient to overcome the binding energy of the cohesion pressure above a critical temperature. Consequently, a body with an interface to the original medium forms from these particles, with the surface energy determining the arrangement of these particles [26].

If the surface area  $A$  of the body is considered and increased by an infinitesimally small value  $dA$ , the work  $dR$  to be done is proportional to this change in area. To increase the surface area, volume work must be performed. This is described by the formula  $dR = -PdV$ , with  $dV$  as the countable volume change by a particle co-volume. In terms of the surface area, this work can also be expressed as  $dR = \alpha dA$ , where  $\alpha$  represents the surface tension, a property given by the van der Waals coefficients. Here  $dA$  is an infinitesimal small area change. This describes the work necessary to increase the surface area of the body. Considering the dimensions of the system components, we must acknowledge that  $A$  is represented by a continuous 2D manifold and  $V$  by a 3D manifold, composed of discrete particles with their own volume that cannot be packed infinitely densely.

Figure 2a shows the isotherms of the van der Waals equation, which allow the formation of interfaces below a critical point. Figures 2b and 2c depict the shapes of the body under the assumption of a continuum and the particle assumption. Since interfaces can only form under the condition of discrete particles with volume, an ideal sphere is excluded. Instead, the particles will seek an arrangement that approximates a sphere and is best described by Goldberg polyhedra [27].

A particular challenge arises in the precise consideration of the boundary of the body, especially when it comes to understanding this boundary as a transition between two different dimensions. The boundary of the body is formed by the outermost particles, which have their own volume and thus represent a volumetric object in three-dimensional space  $\mathbb{R}^3$ . These particles form the surface, which is described as a two-dimensional manifold embedded in three-dimensional space  $\mathbb{R}^3$ . This surface structure requires special consideration, as it is characterized by the interactions between the outermost particles, and the geometry of the surface must be described by the topological and geometric properties of this manifold.

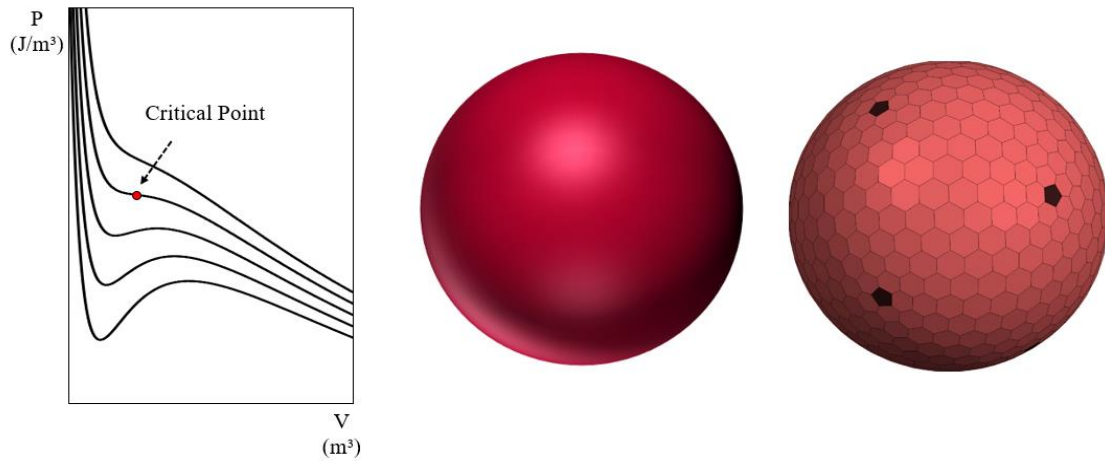


Fig. 2a) Isotherms of the van der Waals equation with the critical point

b) Thermodynamic equilibrium of the continuum

c) Thermodynamic equilibrium of real particles as Goldberg polyhedra

The challenge, therefore, lies in the fact that the interface itself represents an interface where the three-dimensional particles of the body "come into contact" with the two-dimensional surface. This transition structure significantly influences the physical properties of the body and requires precise modeling that correctly considers both the volume structure and the surface structure. When we consider the plasticity index  $\psi$  introduced by Greenwood and Williamson,

$$\psi = \frac{E'}{H} \cdot \sqrt{\frac{\sigma}{\beta}}$$

( $E'$ : Young's Modulus,  $H$ : Hardness,  $\sigma$ : rms Height  $\beta$ : rms Curvature), we can relate the phenomenological properties of elasticity and hardness of the surface to the particle properties  $a$  and  $b$  of the van der Waals equation and consider them as  $\mathbb{R}^3$  properties of the surface due to the volumetric nature of the boundary particles. The second term, on the other hand, describes the statistical properties of a geometric ensemble of randomly distributed coordinates that define the surface area  $A$  of the body.

Since due to the discrete number of particles this description must be approximated by a polyhedral shape, there can be no ideally smooth interface. This transition between smooth Euclidean spaces and fractal structures can be facilitated by Hausdorff measures, which were introduced by Mandelbrot for the description of topographies [28] and used by Zahouani [29] and Bushan [30] for describing tribologically relevant surfaces. Figure 3 shows the hierarchies of the different spaces. While the real

particles of the medium define the body volume and its boundary layer volume at the boundary in  $\mathbb{R}^3$ , the coordinates that define the boundary cannot conform to a smooth norm of  $\mathbb{R}^2$ , but form a fractal structure that is part of the Hausdorff measure  $\mathcal{H}^D$ .

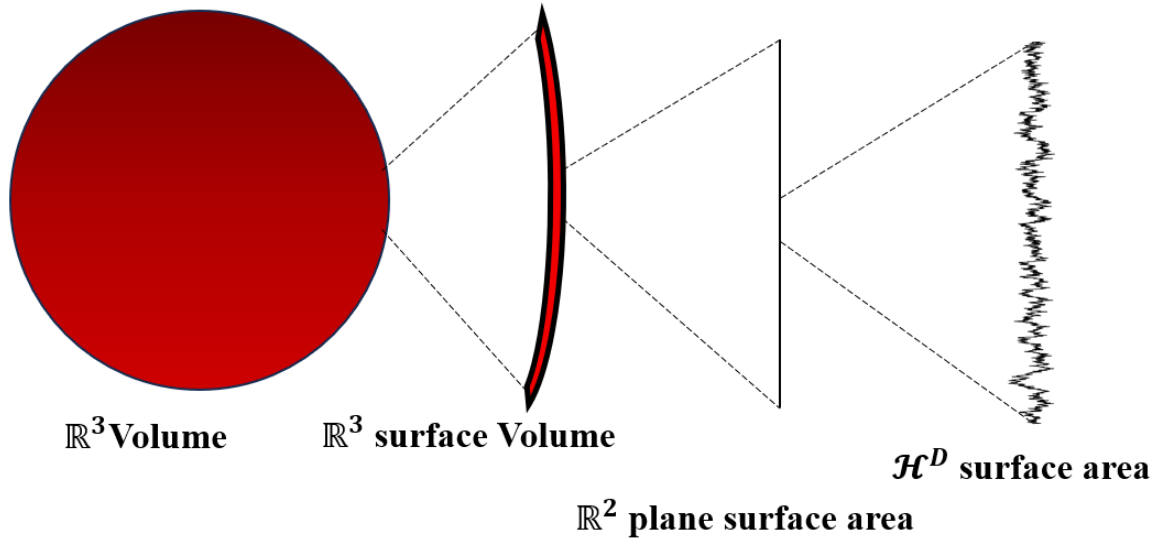


Fig. 3 Hierarchy of metric spaces of an interface and the intermediate measure of fractal dimensions

### 3. Energy of the Coordinate Ensemble of a Topography

To characterize the geometry of a randomly rough surface with fractal dimensions, analogies to its physical properties are demonstrated using statistical physics. Let us consider a continuous ensemble of ordinates  $\zeta_N$ , which are part of the 2-manifold that defines the interface of the body. For each coordinate from  $\zeta_N$ , exactly one degree of freedom  $q_i$  in the embedded dimension  $E$  with the value  $\zeta_i$  exists. Each directly adjacent coordinate possesses the directly adjacent degree of freedom  $q_{i+\delta r}$  with its ordinate value  $\zeta_{i+\delta r}$  such that

$$\|\delta\zeta_i\| = \zeta_{i+\delta r} - \zeta_i$$

represents the difference in ordinate values of two adjacent coordinates and is defined for any arbitrarily chosen metric  $\delta r$ . On any arbitrarily chosen scale for  $\delta r$ , a smallest representable wavelength  $l_s$  can be defined, whose wavelength is determined by the Nyquist-Shannon sampling theorem as twice the distance between two coordinates,  $2\delta r$ . In ISO 21920,  $l_s$  is described as a metrologically meaningful limit where a separation between the roughness signal and shorter wavelength that include amongst other the characteristics of the measuring instrument is possible. The ISO also recommends the use of an L-filter  $l_c$  to achieve a zero-mean topography. The filters are described and interpreted as ideal in the following, so that the evaluation band is unambiguous.

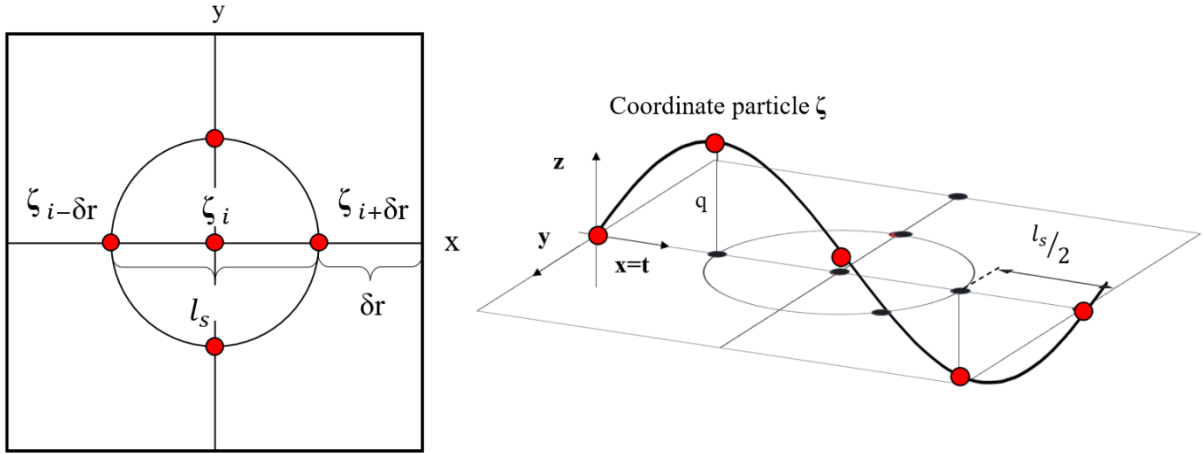


**Fig. 4:** *Left:* Discrete neighborhood of points  $\zeta_i$  with metric  $\delta r$  and the smallest representable wavelength  $l_s$   
*Right:* Continuous wave structure with vertical displacement  $q$  and cutoff frequency  $l_s/2$ , based on the inverse transformation of the PSD(k)

The surface is described using randomly propagating wave vectors. This concept was introduced by Nyak [5] based on the Longuet-Higgins theory for modeling rough topographies with contact mechanical properties. A profile section of the surface with length  $L$  can thus be assembled from a Fourier series. For this purpose, the inverse transformation of a power spectral density PSD(k) of the wave vectors  $\phi = A_k e^{i(kr)}$  with the wave numbers  $k$  up to a smallest representable wavelength  $l_s = L/k_{max}$  with  $k_{max} = L/2 \delta r$  is used. By introducing the measure  $\delta r$ , the necessary number  $N$  of sampling coordinates is obtained with  $N = 1 + L/\delta r$ . To determine the vertical displacement  $\zeta_i$  of the degree of freedom  $q_i$ , the ordinate series  $\zeta_N$  with the random zero-phase  $\theta(k) \in [-\pi; \pi]$  is applied:

$$\zeta_n = \sum_{k=k_{min}}^{N/2} A_k \cdot \cos(k \cdot n - \theta(k))$$

The index  $k$  of the wave numbers starts at a value  $k_{min} = L/l_c$  to emphasize the significance of high wave numbers for surface roughness and to establish formal consistency with the definition of roughness in ISO standards.

The coordinate series  $\zeta_N$  describes the statistical ensemble of all possible sampled surfaces with identical spectral properties of the PSD(k). Figure 4 (left) visualizes the discrete neighborhood relation of the points  $\zeta_i$ , defined by the metric with distance  $\delta r$  and the smallest representable wavelength  $l_s$ . In Figure 4 (right), the continuous representation of the surface as a wave structure is visualized, showing the vertical displacement of the degree of freedom  $q$  along the orthogonal direction  $z$  and the cutoff frequency  $l_s/2$ .

A rough surface is thus understood as a "snapshot" of a moving ocean. Each of these snapshots can be considered a microstate of the statistical ensemble. If the perspective is changed and the vertical displacement of a coordinate  $\zeta_i$  is observed over different time values  $t_0, t_1, t_2, \dots, t_n$  of a period  $T$ , and the temporal intervals  $\delta t$  are scaled in the same metric with  $\delta t = \delta r \cdot T/L$ , then the positions of a coordinate over a period  $T$  are indistinguishable from the positions of coordinates over the length  $L$  measured at a time  $t_0$ . In this scenario, time is to be considered like a lateral spatial coordinate. Thus, the derivative of the ordinate with respect to a lateral spatial coordinate can formally be interpreted as velocity. In Figure 5, the left side shows, as an example, the displacement of a stationary buoy chain at time  $t_0$ , whose vertical displacement is determined by random wave movements. The right side sketches the relation to a time series of a buoy at different time points.

The formation of the gradient in the direction of the x-axis of the randomly rough topography at a time  $t_0$ , which is determined by the differential quotient

$$\frac{d}{dx} \zeta = \frac{\zeta(x + \delta r) - \zeta(x - \delta r)}{2\delta r},$$

can thus be considered analogously to the temporal derivative of a stationary coordinate between two moments  $dt$ :

$$\frac{d}{dt} \zeta(t) = \frac{\zeta(t + \delta t) - \zeta(t - \delta t)}{2\delta t}.$$

The now discrete ordinate values  $\zeta(t_i, x)$  or  $\zeta(x_i, t)$  are defined as  $\zeta_i$ . For the surface of a physical body, it must therefore be assumed that discrete ordinates  $\zeta_i$  with a distance measure  $\delta r$  to their direct neighboring coordinates are present, which simultaneously define half the smallest representable wavelength of a low-pass filter  $l_s$  on each scale and ensure the local smoothness of the topography as a 2-manifold.

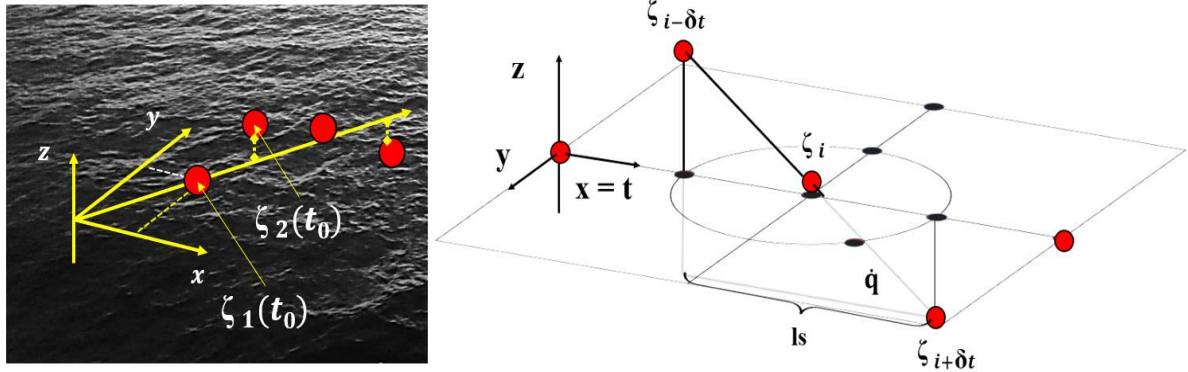


**Fig. 5:** Left: Discrete neighborhood of points  $\zeta_n$  with metric  $\delta r$  and the smallest wavelength  $l_s$

Right: Continuous wave structure with vertical displacement  $q$  and cutoff frequency  $l_s/2$ , based on the inverse transformation of the PSD(k)

Each coordinate of the 2D manifold thus has exactly one degree of freedom  $q$  on any arbitrarily chosen scale in the embedded dimension, and due to the mandatory fractal structure, a gradient, which is formally denoted in its temporal form as  $\dot{q}$ . We want to use these generalized coordinates for the formal description of a topographic energy and begin with the thermodynamic definition of the system energy, which is given by

$$E_S = TS - PV + \mu N.$$

For a body with an interface, the surface energy  $R$  is defined by the particle properties that are forming the surface tension  $\alpha$  and a pure geometrical term.

$$R = \alpha \cdot A.$$

The topographic component of this energy is based solely on properties of the 2D manifold, which forms the surface area  $A$  and does not contain any volume components of the particles or their specific chemical properties. The surface area  $A$  is calculated as is customary in differential geometry, through the integral



$$A = \iint \sqrt{1 + \left(\frac{\delta\zeta_i}{\delta r_x}\right)^2 + \left(\frac{\delta\zeta_i}{\delta r_x}\right)^2} \delta^2 r = \iint \sqrt{1 + \|\nabla\zeta_i\|^2} \delta^2 r.$$

For simplification, the area is reduced to a profile section and only the magnitude for the degree of freedom  $\dot{q}$  of the coordinates in the spatial direction of the profile section with  $\|\nabla\zeta_i\| = \frac{\delta\zeta_i}{\delta r_x}$  is considered. The area, now reduced to the arc length, depends only on the temporal derivative and formally behaves like a kinetic energy  $K$

$$\langle K \rangle = \frac{1}{N} \sum_{i=1}^N \frac{1}{2} m \dot{q}_i^2$$

with  $N$  being the number of sampling points and  $m$  representing a topographic mass, which we want to understand in context of the mass/energy relation  $m = h \cdot \omega / 2\pi \cdot c^2$  where  $h$  needs to be defined with the symplectic differentials of a Hamiltonian system,  $\omega$  is the average weighted roughness frequency and  $c$  represents the acoustic wave speed. Since the topography represents the fractal transition to the smallest possible surface, it is now appropriate to consider the void volume between the maximum and minimum expected values,  $\zeta_{\max}$  and  $\zeta_{\min}$ , of the 2-manifold as another property of the topography. It is immediately noticeable that asymmetric distributions of the coordinates have different void volumes for identical surface areas. Figure 6 shows contour sections of two topographies  $a(x)$  and  $b(x)$  which are represented by a Fourier series with

$$a(x) = d \cdot \cos[(k_{\min} - 2) \cdot x] + \sum_{k=k_{\min}}^{N/2} \frac{l}{k} \cos(kx)$$

$$b(x) = - \left( d \cdot \cos[(k_{\min} - 2) \cdot x] + \sum_{k=k_{\min}}^{N/2} \frac{l}{k} \cos(kx) \right)$$

and whose profile length is identical due to the squaring of the gradient. However, the distribution of the vertical displacement of all coordinates of  $\zeta_N$  is inverted due to the change of algebraic sign. As a

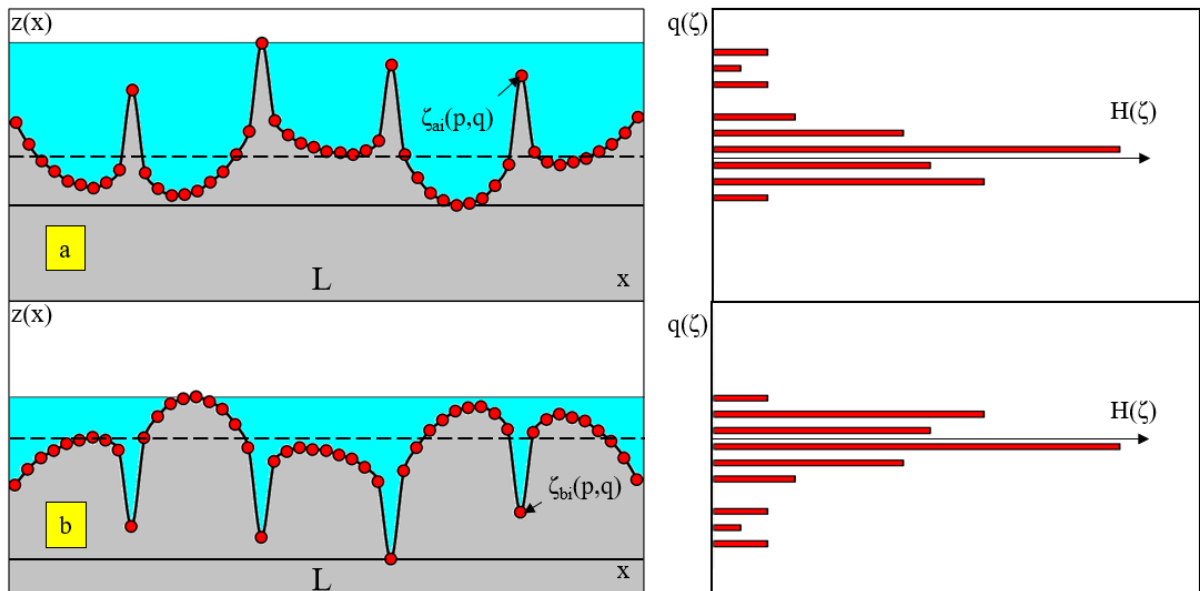


**Fig. 6:** Profile sections  $a$  and  $b$  with identical PSD but inverted amplitudes. A distinction is only given by the distribution of the vertical heights.

topographic potential, the missing volume that the fractal structure lacks compared to the ideally smooth surface is chosen, which depends solely on the degree of freedom  $q$ .

When the void volume of the blue area of the profile sections  $a(x)$  and  $b(x)$  is calculated using the integral of the discrete ordinate values  $\zeta$  and the transfer of the definition  $q_i = \zeta_i - \zeta_{max}$  as the missing volume value of the potential, then the missing position dependent potential Energy  $B$  is given by

$$B = \xi \sum_{i=1}^n q_i \cdot \delta x,$$

with  $\xi$  as a given load or pressure, which we consider the topographic potential and define as the ability of the topography to be filled with plastically deformed material until it reaches the elastic state. It is important that the volume remains independent of the lateral arrangement of the coordinates as long as the topography has a zero mean. Since generalized coordinates  $q_i$  and  $\dot{q}_i$  are used, a Lagrangian function  $L_T$  of the topography can be examined. This is given by the difference between kinetic and potential energy with

$$L_T = \langle K \rangle - B$$

and thus satisfies the equation for the system energy that do not longer contain the van der Waals properties that are stored in the chemical potential  $\mu$  and the countable number of particles  $N$ :

$$E_S = TS - PV.$$

Since this approach considers the surface as a 2-manifold with low pass smoothed Hausdorff dimensions, the volume of individual particles and their attractive forces (which define the chemical potential  $\mu$ ) are assigned to the bulk properties of the body itself. Consequently, van der Waals interactions are not explicitly included in this formulation. Instead, the missing volume  $B$ , together with the load  $\xi$ , forms a mechanical analog to  $PV$ , ensuring a consistent thermodynamic description.

The temperature of a thermodynamic system can be described as a measure of the average kinetic energy of the particles in the system, being proportional to the mean velocity of the particles  $\langle \dot{q} \rangle$  and thus their kinetic energy. By differentiating  $L_T$  with respect to the generalized velocities  $\dot{q}_i$ , a generalized momentum  $p$  can be established by a Legendre Transformation

$$\frac{d}{d\dot{q}_i} L_T = \frac{1}{N} \sum_{i=1}^{N-1} m\dot{q}_i = \frac{1}{N} \sum_{i=1}^{N-1} mp_i$$

leading to a Hamiltonian function:

$$H(p, q) = p_i \dot{q}_i - L_T = \langle K \rangle + B$$

Each coordinate  $\zeta_i$  of a topography ensemble obtains now a defined position in the phase space  $\zeta(q, p)$  through its vertical displacement and its gradient, as shown in Figure 6 for a single coordinate. This allows to demonstrate that the surface energy, defined as  $R = \alpha \cdot A$ , has a topographic component that consists of both the surface area and the void volume, and can be described by a Hamiltonian function. In Figure 7, the different approaches to characterizing a topography as a statistical ensemble are summarized. A contour can be constructed from random numbers as proposed by Whitehouse, and using Monte Carlo simulation it is possible to generate a random series with a given amplitude distribution, from which Mortazevi et al. calculate the Shannon entropy [31]. The PSD provides a comprehensive tool for characterizing topographic information, including fractal dimensions [32]. However, this assumes Gaussian-distributed heights, so that, for example, the changes in vertical structures during

tribological loading, as described by Stout [33], cannot be considered. Describing the surface coordinates as a state in phase space and the resulting definition of a topographic energy via a Hamiltonian function now opens up the possibility of placing surface change processes in a physical context by using both independent statistical properties. We first want to model the case of a run-in surface whose asperities have reached the elastic state. The coordinates of the ensemble can now be understood as uncoupled harmonic oscillators with an average frequency  $\omega$ , whose total energy consists of the sum of their states and can be described by

$$H(p, q) = \frac{1}{2m} \left( \sum_{i=1}^{N-1} p_i^2 + 2\omega^2 \sum_{i=1}^N q_i^2 \right)$$

This could establish a connection to the topographic component from Nosonovsky's generalized Cassie/Wenzel equation [34]. While Nosonovsky shows that the effective contact angle of a surface depends not only on a global roughness factor but must be described by a location-dependent roughness function  $r(x,y)$ , the given approach suggests that this roughness distribution can be supplemented by another inhomogeneous energetic component. In particular, the phase space distribution of the topographic degrees of freedom could be considered as an additional energetic structure that goes beyond the classical concept of macroscopic roughness factors and extends it with another inhomogeneous energetic component.

#### 4. Symplectic Structure of the Topography

The transformation of the topography coordinates into phase space requires the existence of a symplectic structure to define a quantum of action  $h$  and also to avoid possible singularities. We now want to show under which basic conditions a topography fulfills this assumption. An intensive discussion is offered by Chassé in his work 'Hausdorff limits of submanifolds of symplectic and contact manifolds' [35]. Each topographic coordinate  $\zeta_i$  in the configuration space of  $\mathbb{R}^2$  has a neighborhood of direct neighboring coordinates. The fractal dimension allows  $\zeta_i$  exactly one degree of freedom  $q_i$  of location, and the gradient or inclination angle to the direct neighbor corresponds, as explained in the previous chapter, to

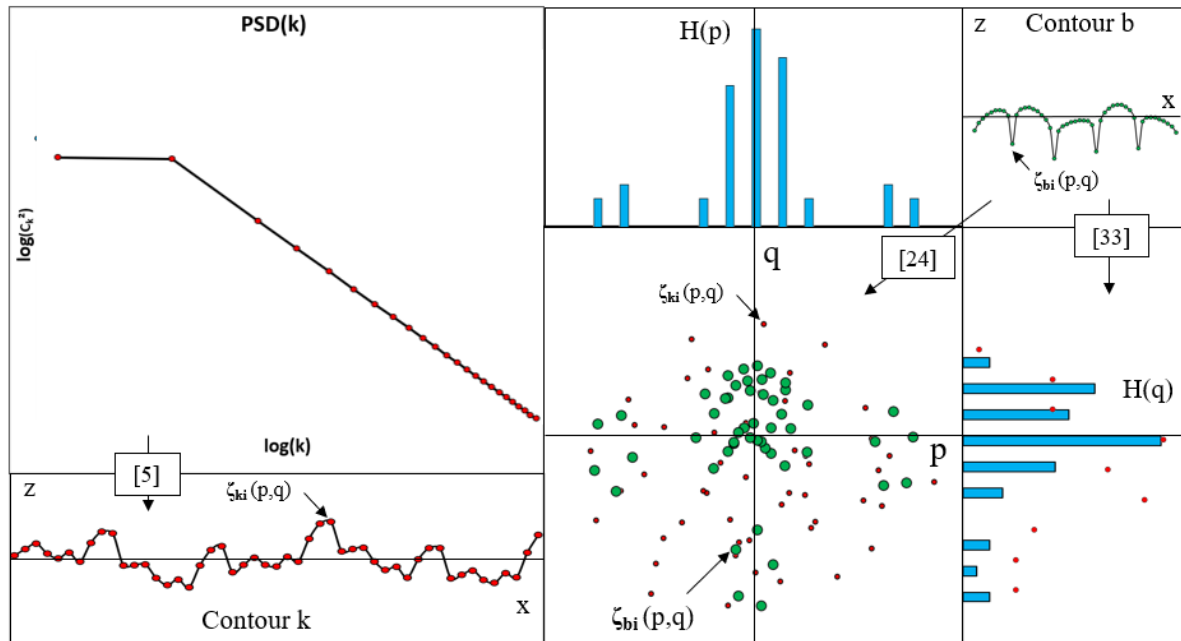


**Fig. 7:** Summary of the relevant statistical properties of a topography that exists as a symplectic structure in phase space. The top left shows the spectral power density of the two contours b and k, which represent two different statistical ensembles. By representing it as an ensemble  $(p,q)$  in phase space, it can be described through energy states. Nayak [5] describes the properties of the PSD of a rough surface, Stout described the role of the height distribution [33] and Brodmann [24] introduced the phase space representation of surface topographies

a 'momentum'  $p_i$ , so that  $\zeta_i$  forms a coordinate pair by itself, which can be assigned an area in phase space that must be formed by differentials  $dp$  and  $dq$  of the canonical coordinates. This would be the fundamental unit of the symplectic structure and ensures that the space can be described statistically and geometrically meaningfully, as the product  $dpdq$  must be non-zero and represents the quantum of action  $h$ .

Due to the fractal dimensions of the topography, there is no smooth manifold in the configuration space. Only the definition of a smallest representable wavelength allows for a physically meaningful scale. To calculate the differentials  $dq$  and  $dp$ , we use the rms value of the ensemble  $\zeta_N$ , which is referred to as  $Rq$  in the roughness norm and which we initially interpret as the standard deviation of a normal distribution.

$$\sigma = \sqrt{\langle \zeta_N^2 \rangle - \langle \zeta_N \rangle^2}$$

What is required is a method that defines a class width derived from measure theory. For this, 'Scott's Rule' is suitable, which derives this from the minimization of the integrated mean squared error (IMSE) for a sample size  $N$  with a standard deviation  $\sigma$  [36].

$$cw_q = dq = \frac{\varepsilon \cdot \sigma}{\sqrt[3]{N}}$$

( $\varepsilon$ : scaling factor with 3.49 for the normalized Gaussian distribution,  $\sigma$ : the rms-value of  $q(\zeta_N)$ ,  $N$  the number of information bearing coordinates and the procedure for  $cw_p$  is its vice versa). Since the basic assumption for randomly rough surfaces is a normal distribution of heights values, we choose  $\varepsilon$  to be 3.49, independent of the actually measured statistical distribution. The class width  $cw_q$  of the verticals is defined as  $dq$  and  $dp$  for the classwidth  $cw_p$  of the symplectic structure. Now an expression for  $h$  as a limit of the phase space is available.

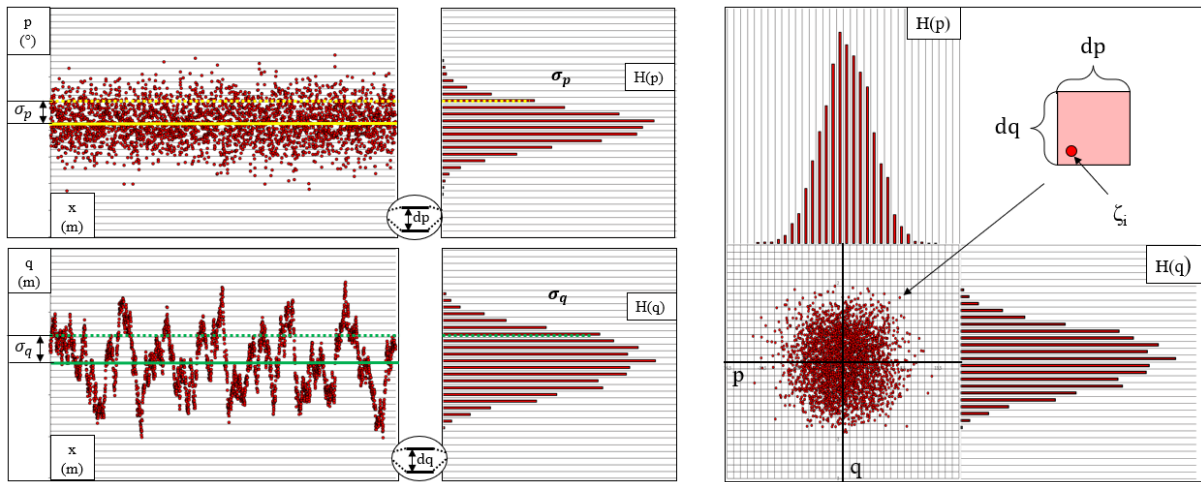


**Fig. 8:** Visualization of the phase space transformation of topography coordinates, illustrated by the representation of the angles  $p$  and positions  $q$  along the  $x$ -axis. The histograms  $H(p)$  and  $H(q)$  shown on the right display the distributions of the corresponding values, while the scatter plots illustrate the dynamic distribution in phase space. The differentials  $dp$  and  $dq$ , represented by the red areas, serve to define the symplectic structure and enable a geometrically and statistically meaningful description of the space.

To derive a number of classes in addition to the class width that defines the possible location of a coordinate as a state, a stable measure for the event space of the vertical states. For statistically rough surfaces, Seewig offers an approach: He shows that knowing a standard deviation  $\sigma$  and a number of sampling points  $N_{lc}$  provides a stable idea of the resulting space  $\Omega(q)$  in which a coordinate can be found [37], provided the type of amplitude density distribution function is known. Since roughness is defined as a quantity that represents deviations from the smooth Euclidean norm of  $\mathbb{R}^2$ , the geometrically meaningful spatial frequencies are reduced by applying an L-filter. This avoids misinterpretations by

more complex geometric bodies. Using numerical integration, an expected value for the possible values of  $q$  can be estimated according to Seewig as the difference between  $q_{max}(\text{peak})$  and  $q_{min}(\text{valley})$  from the standard deviation and the number of sampling points  $N_{lc}$ .

The statistical structure of a rough surface can thus be described by the distribution of its degrees of freedom in both position and momentum space. Figure 8 illustrates, at the bottom left, the distribution of the degrees of freedom  $q_i$  of the ensemble  $\zeta_N$  at a defined time  $t_0$  as well as the corresponding histogram  $H(q)$ . The class width  $dq$ , derived from the standard deviation  $\sigma_q$  and the number of sampling points  $N$ , illustrates the statistical discretization of the vertical displacements.

The ensemble is shown in the momentum space in the upper left part of the diagram, with a corresponding histogram  $H(p)$  and the calculated class width  $dp$ . Both distributions, in position and momentum space, are embedded in the phase space on the right side of the figure, where they are bounded by the symplectic units  $dq$  and  $dp$ . This representation makes it clear that each coordinate  $\zeta_i$  of the ensemble  $\zeta_N$  occupies a well-defined position in phase space through its vertical displacement  $q_i$  and its momentum  $p_i$ , which is bounded by the differentials  $dq$  and  $dp$ . This area represents a subsystem that can be examined in detail on a smaller scale. The coordinate ensemble itself represents a possible microstate in which the topography has comparable functional properties.

For the ensemble, the phase space volume can be calculated. To do this, the fact that the density distributions of position and momentum coordinates are statistically independent is used. Thus, the phase space volume  $\Omega(\Delta p_i, \Delta q_i)$  of an area is calculated with its relative occupancy frequency and the number of meaningful coordinates  $N$  as

$$\Omega(\Delta p_i, \Delta q_i) = N \cdot H(p_i) \cdot H(q_i) \cdot \Delta p_i \Delta q_i$$

and can be summed over the entire possible event space as

$$\Omega(\Delta p, \Delta q) = N \cdot \sum_{i=1}^{n_p} \sum_{j=1}^{n_q} H(p_i) \cdot H(q_j) \cdot \Delta p_i \Delta q_j.$$

The calculation of the Entropy of the ensemble follows as

$$S = k \cdot \ln \Omega(\Delta p, \Delta q)$$

which gives us the entropy of a microstate, namely that of the measurement of the statistical ensemble.

The topographic information of a surface thus gives us one of the many possible microstates that the coordinate ensemble can occupy. At the same time, we must accept that slight variations in the statistical properties of the microgeometry of a macroscopic geometric body are permissible 'fluctuations' of an otherwise homogeneous state [26]. Inhomogeneities in the statistical characteristics are therefore mandatory statistical properties that must be characterized metrologically through a sufficiently large number of samples.

## 5. Topographic Energy in Tribological Applications of a Two-Disk Test Rig

By introducing a Hamiltonian for a topography ensemble, mechanically induced geometric changes of the surface can be interpreted in a thermodynamic context. This is illustrated by an experiment conducted at the Center for Microtribology as part of the TriboKon project (FKZ 22004618) [38]. In this experiment, two ground rollers, one cylindrical (disk) and one crowned (pin), both made of 16MnCr5 case-hardened steel ( $60 \pm 4$  HRC), were examined. The rollers operated in a two-disk test rig under lubrication with an oil of viscosity class ISO VG 32, which had a temperature of  $50^\circ\text{C}$  at the time of supply. The general operating principle of the test rig is described in [39].

The contact area was subjected to high surface pressure (2 GPa) and low sliding speed for 70 hours. The coefficient of friction was determined at five different points in time [38]. Figure 9 outlines the principal setup: On the left, the cross-sections of the two rollers and the viewing direction for the right image area

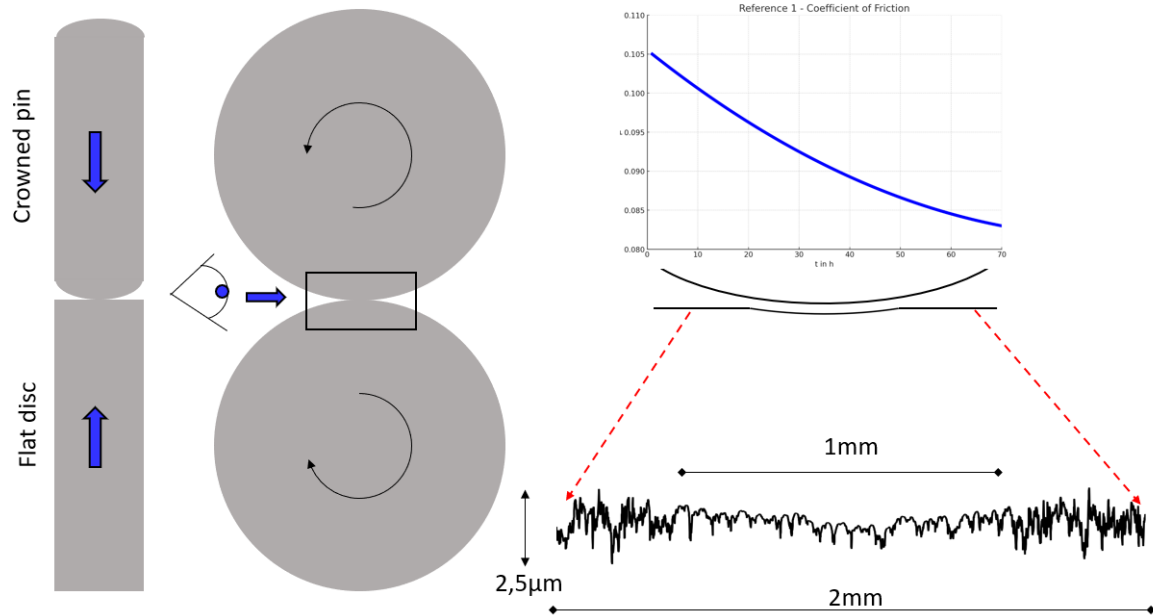


**Fig. 9:** Experimental setup of the two-disc test rig.

are shown. On the right, the contact area of the crowned roller after the final run is depicted as a qualitative profile section. The smoothing of the running-in track and the plastic deformation of the contact ellipse are clearly visible in the measurement. The top right graphic shows the measured coefficient of friction over the test duration of 70 hours. It decreases almost constantly from 0.105 to 0.082.

The change in the microtopography of the flat test specimen before and after the tribological run-in is measured using a multi-pinhole confocal microscope from NanoFocus [40] and a scatter-o-meter from OptoSurf and the resulting information is used to apply the model introduced in the previous chapters for an interpretation of the tribological process. The scatter-o-meter is an advancement of the setup described by Brodmann et al. in [41] and transfers the light beams reflected by the surface microgeometry to a detector using Fourier optics, where the distribution of light flux intensity over the reflection angles is measured. While confocal microscopy represents a suitable method for measuring the vertical properties and their statistical distribution, scatterometry can describe the distribution of surface angles on a defined scale, as the measurement principle is based on the mirror facet model of Torrence/Sparrow [42], and Brodmann and Allgäuer were able to prove its validity even for small roughnesses [43]. The normalized intensity distribution of the light can be directly interpreted as the frequency distribution of the topography angles. Seewig describes this model in [44] from a systems theory perspective. Eifler et al. show in [45] that the measurements can be traced back to SI units and calibrated with bespoke material measures. Feidenhansl et al. demonstrate in [46] that the setup conforms to classical scattered light methods and show the relationship between surface angles and spatial frequencies, so that a shortest representable wavelength  $l_s$  can also be calculated for this instrument, which is given by the numerical aperture of the Fourier optics. Feidenhansl et al. specify a shortest representable wavelength of  $2.4 \mu\text{m}$  for the rBRDF instrument, making this device very suitable for the scale of microgeometry described as roughness by international standards [47]. The scatterometer directly measures the distribution of angles and the parameters that can be calculated from the distribution. For the second statistical moment the parameter is called  $Aq$ , where “A” is representing angle. It is directly proportional to the rms slope  $Rdq$

$$Aq = 4kR\Delta q^2$$

(k:1.17 defines  $Aq = 100$  for a rectangular distribution).

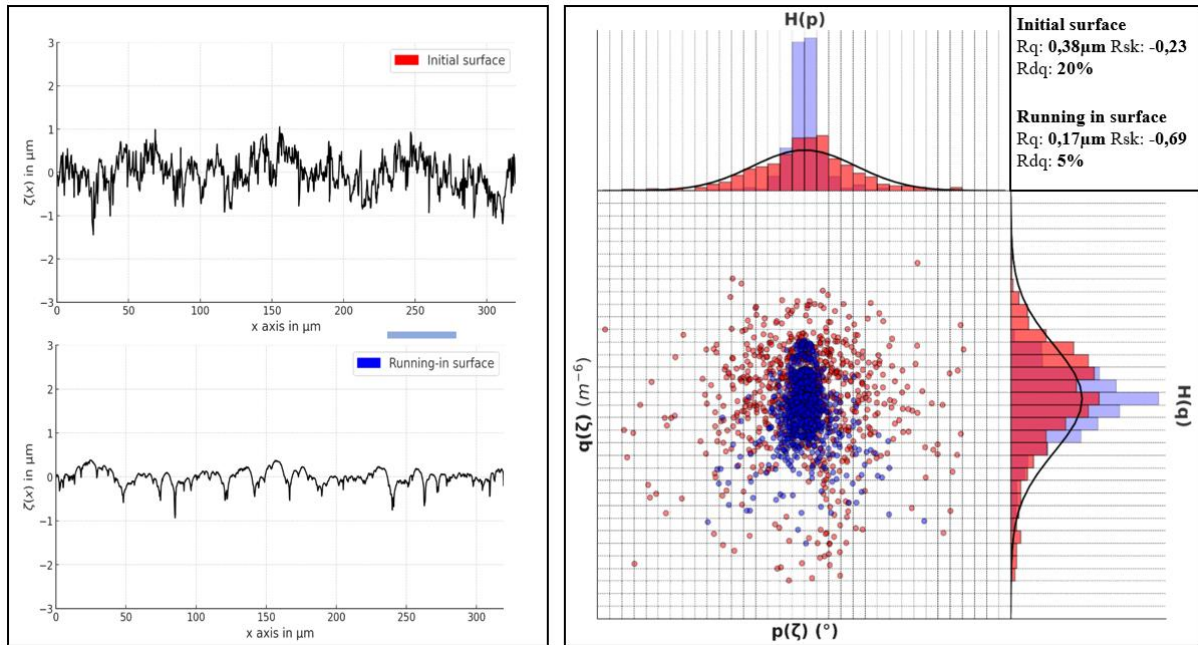


**Fig. 10:** Comparison of Surface Characteristics: Top left shows the initial surface and below it the run-in surface, depicted as height profiles depending on the x-axis. On the right, the distribution analysis of the surfaces in phase space is shown through the generalized coordinates  $p(\zeta)$  vs.  $q(\zeta)$  with the corresponding histograms of the derivatives  $H(p)$  and the ordinates  $H(q)$ , and the basic condition in the form of a normal distribution for the probability space.

A combination of the information of the two measurement approaches allows the direct determination of the distribution of both height values and the surface gradients, leading to a phase space representation and comprehensive interpretation of the tribological process. Since topographically measuring systems generate large uncertainties within the numerical derivation of height values, they are only limitedly suitable for measuring gradient information. By combining the two physical measurement methods, functional properties can be directly considered from an energetic perspective. First, the topographies of the samples 'Initial Surface' and 'Running-in Surface' were recorded confocally with a 50x objective NA 0.8 over an area of  $320\mu\text{m} \times 320\mu\text{m}$ . The application of a first and second-order F-operator initially eliminates long-wavelength form components. Subsequently, the high-frequency spatial frequencies, which are associated with large uncertainties, were limited by applying the S-filter operation with a cutoff wavelength of  $2.5\mu\text{m}$ , thus defining a meaningful metric  $dr$  of  $1.25\mu\text{m}$ . Over an area of  $(320\mu\text{m})^2$ , this would result in 65,536 information-bearing coordinates. Following Nosonovski's reasoning [34], however, we interpret the triple point line represented by a profile section as carrying information. Due to the smallest representable wavelength, the additional information located within the measurement field from a higher point density can thus only be interpreted as fluctuations of roughness inhomogeneities. The profile sections shown in Figure 10 are therefore directly equated with the triple point or three-phase line of the generalized Cassie/Wenzel equation, allowing us to find a more general definition for calculating the number of information-bearing coordinates and to calculate a resulting class width for the differentials  $dq$  and  $dp$  of the symplectic structure. To identify the number of information-bearing points, again the considerations of Seewig [37] are used to obtain an order of magnitude of  $10^3$  for a typical line measurement of 4 mm at a probability limit of  $\pm 4\sigma$ , assuming a normal distribution as the natural case. We measure the rms roughness at  $0.38\mu\text{m}$  and obtain an expected maximum range of  $3.04\mu\text{m}$ . Applying Scott's Rule results in a class width of 0.09 and a number of 34 classes. We proceed identically with the ordinate values numerically derived using the 3-point rule.

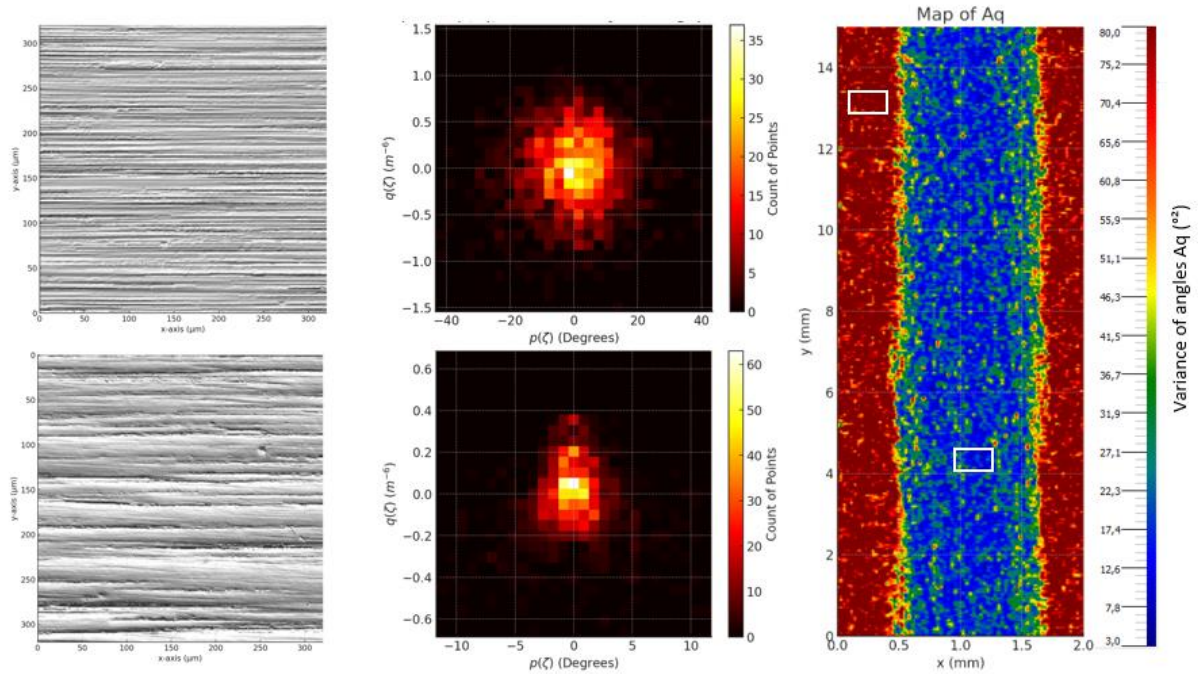


**Fig. 11:** left: Topography images of the initial and running in surface; middle: Phase space representation of the topographical ensembles; right: colour map of the local  $Aq$  variations of the reference sample measured by an OS500 scatter o meter with a spot size of  $30\mu\text{m}$ .

Through the class widths, the topographic energy states are identified via the symplectic differentials. Now, we can assign each coordinate a location in phase space, as seen in the right diagram of Figure 10. Comparing the change in the run-in topography with the original, we observe the changes in statistical moments described in the literature [33]. A lower rms value and an increasing negative skewness can be observed. However, the most significant change is seen in the decrease of the mean gradient. On the one hand it shows the significance of the root mean square gradient and on the other this illustrates how meaningful the representation in the phase space is: there are tribological processes that do not majorly change the statistical distribution of height values but have a significant impact on the angular distribution. Thus, but monitoring both quantities, even slightest changes in the surface topography can be detected, visualized and monitored in the phase space representation. Changes that cannot be mapped by the monitoring of profile or areal surface texture parameters are observable in the phase space representation. The statistical moments are the observables of the surface microstructure states and are independent from the structure properties of one single microstate. The new picture of the phase space representation emerges from the combination of the two density distributions and allows an interpretation of surface changes using a comprehensive perspective. In Figure 11, the left side shows

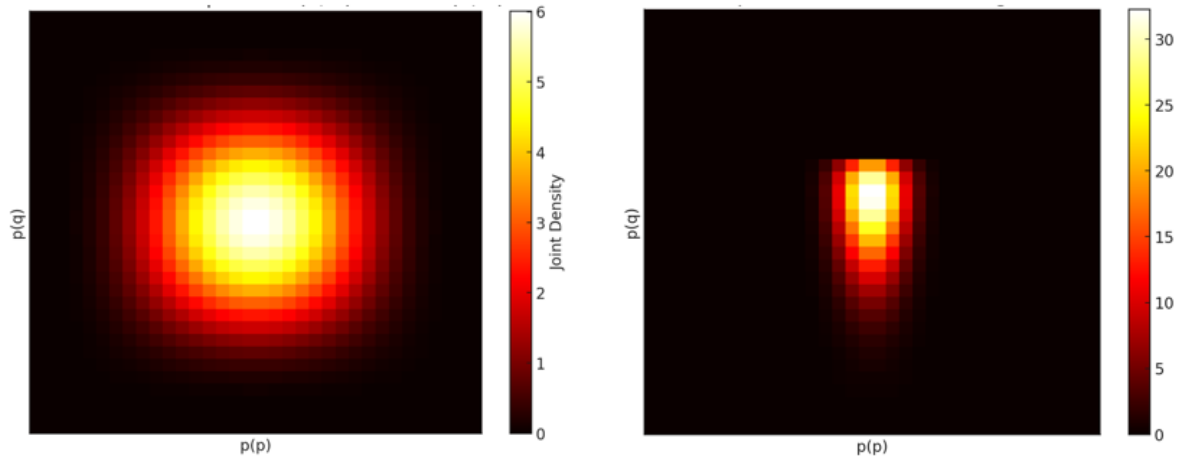


**Fig. 12:** simulations of surface topography “wavefunctions” using the joint Beta distribution. Left: Initial surface, Right: running in surface.



the confocal topography image of the initial and run-in surfaces. In the middle, their resulting phase space density is visualized. The different scaling of the phase space images should be noted. The right part of the image shows the scatterometer measurement and the colour map of 7,000 single  $Aq$  values.

For a more general case the idea of Zheng and Whitehouse in [48] can be applied by defining a bivariate function that can be expressed as a surface roughness “Wavefunction”, by combining e.g. the Beta distribution of two independent Variables  $p$  and  $q$  to a joint distribution  $\psi(p, q)$ . The Beta distribution is a common density function in surface metrology [48] can be expanded to

$$\psi(p, q) = \frac{(p)^{\alpha_p-1}(1-p)^{\beta_p-1}}{B(\alpha_p, \beta_p)} \cdot \frac{(q)^{\alpha_q-1}(1-q)^{\beta_q-1}}{B(\alpha_q, \beta_q)}$$

$\alpha_p, \alpha_q$  and  $\beta_p, \beta_q$  are the coefficients that are describing the shape of the distribution and  $B(\alpha, \beta)$  is the Betafunction. This Joint distribution function can be used to investigate the behavior of topographical changes in tribological systems during the applied load. As the normalized Beta-distribution is used, the function needs to be rescaled. In Figure 12 the simulated joint distributions for an initial and a running in surface are shown.

The running-in surface has significantly fewer occupied states in both, the simulation and the experiment and a clear accumulation of states near the phase space origin can be observed. In the language of statistical physics, this corresponds to a reduction in entropy along with a simultaneous loss of energy. This process can formally be interpreted as the formation of a dissipative structure in the sense of a self-organization process and supports Nosonovski's argument of assigning entropy and energy properties to the topography with a geometric structure [49]. This opens up the possibility of considering tribological processes in a GENERIC formulation, as used by Oettinger in his nonequilibrium thermodynamics for rheological systems [50]. This model can be applied for more real tribological system to improve the efficiency of machine elements.

As shown, the challenge of quantification changes of tribological arises from the large measurement uncertainties of topographically measuring systems when evaluating surface inclinations. A necessary complement here is the scattering light method described in VDA2009 [51]. Through the direct measurement of the angular distribution, high measurement speed, and robustness against disturbances, a full-surface measurement is possible, and inhomogeneities can be observed as it is shown in Figure 13. The measurement of the phase-space using both topographic and angular information by a combination of surface texture and angular scattering measurement opens a wide new field for

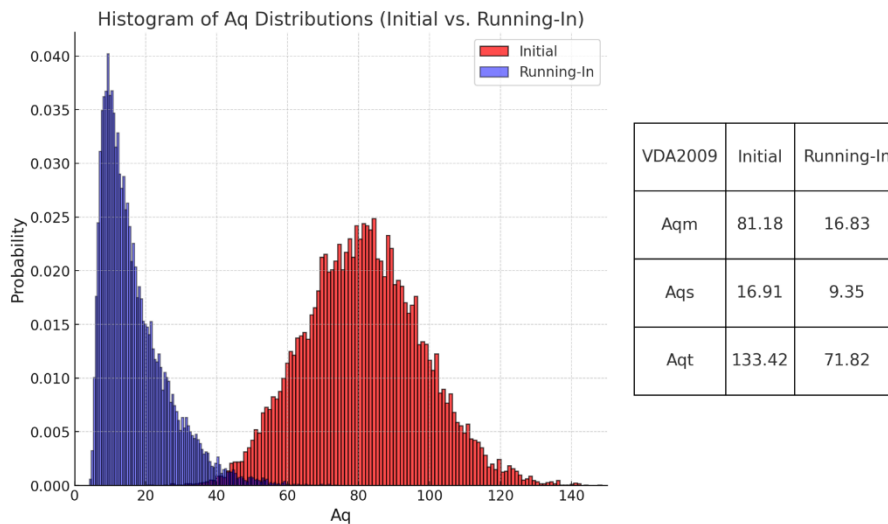


**Fig. 13:** Surface statistics of inhomogeneities before and after the load test.  $Aqm$  is the average,  $Aqs$  the standard deviation and  $Aqt$  is the Range of values. A parameter description can be found in VDA2009 [51]

investigations of surface characteristics that are not considered so far and can enhance the monitoring and interpretation of tribological processes.

## 6. Summary & Conclusion

To assess tribological processes, the monitoring and interpretation of the state of a surface is a key activity which is however most commonly limited to the determination of topography height values and associated surface texture parameters. The surface should however be interpreted more generically to provide possibilities for a comprehensive assessment of tribological processes.

From phenomenological thermodynamics a distinction between two-dimensional and three-dimensional manifolds of tribologically effective surfaces can be derived, and the general existence of fractal dimensions on the surface of physical bodies can be demonstrated. Using the smallest representable wavelength, a coordinate ensemble with a metric  $dr$ , where each coordinate possesses a generalized degree of freedom  $q$  and a differential amount  $dq$  relative to its neighbor across every scale of fractal dimension could be identified.

The resulting metric can be interpreted as a time coordinate, which subsequently allows the derivative of the generalized coordinate  $q$  to be interpreted as velocity  $\dot{p}$ . From a geometric dimension analysis, a topographic Lagrangian can be determined and transformed into a Hamiltonian through the application of generalized momentum. Each coordinate of the ensemble possesses its own coordinate pair that assigns it to a location in phase space.

With the aid of statistical considerations, a symplectic structure  $dpdq$  and the phase space volume can be defined. Through a two-disc experiment, it was demonstrated that changes in topography under load can be understood as a self-organization process through thermodynamic reasoning. The application of a joint distribution allows to define a wave function of topography, which is suitable for characterizing the topography.

For quantification, we propose the use of topographic measuring systems in combination with a scattered light method, allowing for a reliable measurement of both the surface topography and the surface inclinations and the quantification of inhomogeneities. This methodological approach for a direct measurement of a phase space representation of the surface topography offers a sophisticated tool for examining the complex interactions at the surface, providing insights that are crucial for optimizing material performance in tribological applications. In future work, further examinations of the approach using different use-cases will be conducted to gain additional insights into the application of the phase space representation for the monitoring and assessment of tribological processes in industrial applications.

## Acknowledgement

We would like to thank Dominik Linsler (Fraunhofer MicroTribology Centrum  $\mu$ TC) and Florian Reinle (OTEC Precision Finishing Solutions) for the experimental data of the two-disc test stand. Furthermore, we would like to thank Poul-Erik Hansen (Danish National Metrology Institute DFM), Jörg Seewig (RPTU Kaiserslautern-Landau), Dorothee Hüser (German National Metrology Institute PTB), Maximilian Kohris (RPTU Kaiserslautern-Landau) for their support and openness to discuss some of the presented concepts.

## References:

- [1] Vincent Coll, & Michael Harrison. (2014). Gabriel's Horn: A Revolutionary Tale. *Mathematics Magazine*, 87(4), 263–275. <https://doi.org/10.4169/math.mag.87.4.263>
- [2] Bekenstein, J. D. (1973). Black Holes and Entropy. *Physical Review D*, 7(8), 2333–2346. DOI: 10.1103/PhysRevD.7.2333
- [3] Gesellschaft für Tribologie e.V.: Arbeitsblatt 7 Tribologie. Definitionen, Begriffe, Prüfung. Eigendruck der GfT e.V., Moers, 2002
- [4] J.A. Greenwood, J.B.P. Williamson, contact of nominally flat surfaces, Proc. R. Soc. Lond., 12/6 1966. <https://doi.org/10.1098/rspa.1966.0242>
- [5] Nayak, P.R. Random Process Model of Rough Surfaces. *J. Lubr. Technol. (ASME)* 1971, 93, 398–407
- [6] Whitehouse, D.J.; Archard, J.F. The Properties of Random Surfaces of Significance in Their Contact. Proc. R. Soc. Lond. A Math. 1970, 316, 97–121
- [7] Persson, B. N. J. (2001). *Theory of rubber friction and contact mechanics. The Journal of Chemical Physics*, 115(8), 3840–3861. doi:10.1063/1.1388626
- [8] J.J. Gagnepain, C. Roques-Carmes, Fractal approach to two-dimensional and three-dimensional surface roughness, *Wear*, Volume 109, Issues 1–4, 1986, Pages 119-126, ISSN 0043-1648, [https://doi.org/10.1016/0043-1648\(86\)90257-7](https://doi.org/10.1016/0043-1648(86)90257-7).
- [9] D.J. Whitehouse, Fractal or fiction, *Wear*, Volume 249, Issues 5–6, 2001, Pages 345-353, ISSN 0043-1648, [https://doi.org/10.1016/S0043-1648\(01\)00535-X](https://doi.org/10.1016/S0043-1648(01)00535-X).
- [10] Persson, B. N. J., Albohr, O., Tartaglino, U., Volokitin, A. I., & Tosatti, E. (2005). On the nature of surface roughness with application to contact mechanics, sealing, rubber friction and adhesion. *Journal of Physics: Condensed Matter*, 17(1), R1-R62. <https://doi.org/10.1088/0953-8984/17/1/R01>
- [11] N.O.Myers: Characterization of surface roughness, *Wear* Volume 5, Issue 3, May–June 1962, Pages 182-189, [https://doi.org/10.1016/0043-1648\(62\)90002-9](https://doi.org/10.1016/0043-1648(62)90002-9).
- [12] Hyun S, Pei L, Molinari JF, Robbins MO. Finite-element analysis of contact between elastic self-affine surfaces. *Phys Rev E Stat Nonlin Soft Matter Phys*. 2004 Aug;70 (2 Pt 2):026117. doi: 10.1103/PhysRevE.70.026117. Epub 2004 Aug 31. PMID: 15447555
- [13] Popov, V. L., & Pohrt, R. (2016). *What does friction really depend on? Robust governing parameters in contact mechanics and friction. Mechanics of Solids*, 51(2), 123–127. DOI: 10.1134/S1029959916020016
- [14] Whitehouse, D. J. (2012). *Handbook of Surface and Nanometrology* (2nd ed.). CRC Press. DOI: 10.1201/b12956
- [15] Pfeffer, P., & Harrer, M. (2011). *Lenkungshandbuch: Lenksysteme, Lenkgefühl, Fahrdynamik von Kraftfahrzeugen*. Springer Vieweg. <https://doi.org/10.1007/978-3-658-00977-9>
- [16] Brodmann, B., & Bodschwinn, H. (2019). Scattered light measurement on worm gears with high efficiency requirements. In *Proceedings of the International Conference on Gears 2019*

- (S. 1567–1578). VDI Verlag. <https://doi.org/10.51202/9783181023556/international-conference-on-gears-2019>
- [17] Jacobs, T. D. B., Pastewka, L., & Müser, M. H. (2022). Surface topography as a material parameter. *MRS Bulletin*, 47(9), 635–642. <https://doi.org/10.1557/s43577-022-00465-5>
- [18] Prigogine, I., & Lefever, R. (1977). *Self-Organization in Nonequilibrium Systems: From Dissipative Structures to Order Through Fluctuations*. Wiley-Interscience.
- [19] Scherge, M. The Running-in of Lubricated Metal-Metal Contacts—A Review on Ultra-Low Wear Systems. *Lubricants* 2018, 6, 54. <https://doi.org/10.3390/lubricants6020054>
- [20] Archard, J.F. Elastic Deformation and the Laws of Friction. *Proc. R. Soc. Lond. A Math.* 1957, 243, 190–205.
- [21] Godet, M. (1984). The Third-Body Approach: A Mechanical View of Wear. *Wear*, 100(4), 431–452. [https://doi.org/10.1016/0043-1648\(84\)90025-5](https://doi.org/10.1016/0043-1648(84)90025-5)
- [22] Nosonovsky, M. (2010). Entropy in Tribology: in the Search for Applications. *Tribology Letters*, 38(1), 65–75. <https://doi.org/10.1007/s11249-010-9676-6>
- [23] Carcassi, G., Aidala, C. A., & Barbour, J. (2021). Variability as a better characterization of Shannon entropy. *European Journal of Physics*, 42(4), 045102. <https://doi.org/10.1088/1361-6404/abe361>
- [24] Brodmann, B. (2024). *Charakterisierung tribologischer Funktionsflächen im Phasenraum*. Tribologie und Schmierungstechnik, Band 70, Sonderausgabe 2, eOnly. Narr Verlag, Tübingen. ISBN: 978-3-381-10202-0.
- [25] Peklenik, J. (1967). New developments in surface characterization and measurements by means of random process analysis. *Proceedings of the Institution of Mechanical Engineers*, 182(1), 309–320. [https://doi.org/10.1243/PIME\\_CONF\\_1967\\_182\\_309\\_02](https://doi.org/10.1243/PIME_CONF_1967_182_309_02).
- [26] Landau, L. D., & Lifshitz, E. M. (2016). *Statistische Physik, Teil 5* (8. Aufl.). Akademie-Verlag.
- [27] Goldberg, M. (1937). A class of multi-symmetric polyhedra. *Tohoku Mathematical Journal*, 43, 104–108.
- [28] Mandelbrot, B. (1967). How Long Is the Coast of Britain? Statistical Self-Similarity and Fractional Dimension. *Science*, 156(3775), 636–638. <http://www.jstor.org/stable/1721427>
- [29] Zahouani, H., Vargiolu, R., & Loubet, J.-L. (1998). Fractal models of surface topography and contact mechanics. *Mathematical and Computer Modelling*, 28(4–8), 517–534. [https://doi.org/10.1016/S0895-7177\(98\)00139-3](https://doi.org/10.1016/S0895-7177(98)00139-3)
- [30] Ganti, S., & Bhushan, B. (1995). Generalized fractal analysis and its applications to engineering surfaces. *Wear*, 180(1995), 17–34. [https://doi.org/10.1016/0043-1648\(94\)06545-4](https://doi.org/10.1016/0043-1648(94)06545-4)
- [31] Mortazavi, V, Menezes, PL, & Nosonovsky, M. “Studies of Shannon Entropy Evolution due to Self-Organization During the Running-In.” Proceedings of the ASME/STLE 2011 International Joint Tribology Conference. ASME/STLE 2011 Joint Tribology Conference. Los Angeles, California, USA. October 24–26, 2011. pp. 303–305. ASME. <https://doi.org/10.1115/IJTC2011-61231>
- [32] Tevis D B Jacobs *et al* 2017 *Surf. Topogr.: Metrol. Prop.* **5** 013001 DOI 10.1088/2051-672X/aa51f8

- [33] Stout, K. J., King, T. G., & Whitehouse, D. J. (1977). Analytical techniques in surface topography and their application to a running-in experiment. *Wear*, 43(1), 99–115. [https://doi.org/10.1016/0043-1648\(77\)90046-1](https://doi.org/10.1016/0043-1648(77)90046-1).
- [34] Nosonovsky, M. (2007). *On the range of applicability of the Wenzel and Cassie equations*. *Langmuir*, 23(19), 9919–9920. <https://doi.org/10.1021/la701324m>
- [35] Chassé, J.-P. (2024). Hausdorff limits of submanifolds of symplectic and contact manifolds. *Differential Geometry and its Applications*, 94, 102123. <https://doi.org/10.1016/j.difgeo.2024.102123>
- [36] David W. Scott, On optimal and data-based histograms, *Biometrika*, Volume 66, Issue 3, December 1979, Pages 605–610, <https://doi.org/10.1093/biomet/66.3.605>
- [37] Seewig, J. (2013): The uncertainty of roughness parameters. In: *Proceedings of SENSOR 2013*, AMA Conferences, S. 2912–2962. DOI: 10.5162/sensor2013/B6.2
- [38] Reinle, F., & Linsler, D. (2023). Reibungsoptimierung durch Gleitschleifen: Das Einlauf- und Reibverhalten über Topographie einstellen. In M. Jungk, M. Wittmaack, & M. A. Markus (Hrsg.), *Tribologie und Schmierungstechnik*, 70(3).
- [39] Grebe, M. (2012). Model tests with a modern two-disc test rig as an alternative to expensive gearbox tests. Presentation, March 2012. DOI: 10.13140/RG.2.2.23356.51849
- [40] Brodmann, R. (2005). *Surface metrology of engineering surfaces by means of the multi-pinhole technique*. *Insight - Non-Destructive Testing and Condition Monitoring*, 47(4), 232–235. <https://doi.org/10.1784/insi.47.4.232.63158>
- [41] R. Brodmann *et al.*, "An optical instrument for measuring the surface roughness in production control," *CIRP Annals*, vol. 33, no. 1, pp. 403–406, 1984. doi:10.1016/S0007-8506(07)61451-6
- [42] Cook, R. L., & Torrance, K. E. (1981). *A Reflectance Model for Computer Graphics*. *Computer Graphics (Proceedings of SIGGRAPH '81)*, 15(3), 307–316. <https://doi.org/10.1145/800224.806819>
- [43] R. Brodmann and M. Allgauer "Comparison Of Light Scattering From Rough Surfaces With Optical And Mechanical Profilometry", *Proc. SPIE 1009, Surface Measurement and Characterization*, (21 March 1989); <https://doi.org/10.1117/12.949161>
- [44] Seewig, J., Beichert, G., Brodmann, R., Bodschwinn, H., & Wendel, M. (2009). *Extraction of Shape and Roughness using Scattering Light*. *Proceedings of SPIE*, 7389, 7389-24. <https://doi.org/10.1117/12.827478>
- [45] Eifler, M., Brodmann, B., Hansen, P. E., & Seewig, J. (2021). *Traceable functional characterization of surface topography with angular-resolved scattering light measurement*. *Surface Topography: Metrology and Properties*, 9(3), 035042. <https://doi.org/10.1088/2051-672X/ac2031>
- [46] Feidenhans'l, N. A., Hansen, P.-E., Pilný, L., Madsen, M. H., Bissacco, G., Petersen, J. C., & Taboryski, R. (2015). Comparison of optical methods for surface roughness characterization. *Measurement Science and Technology*, 26(8), Article 085208. <https://doi.org/10.1088/0957-0233/26/8/085208>
- [47] ISO 25178-3: Geometrical product specifications (GPS) - Surface texture: Areal - Part 3: Specification operators (ISO 25178-3:2012)

- [48] Whitehouse, D J/K G Zheng (1992): The use of dual space-frequency functions in machine tool monitoring, in: *Measurement Science and Technology*, vol. 3, no. 9, pp. 796–808, [online] doi:10.1088/0957-0233/3/9/002.
- [49] Grmela, M., & Öttinger, H. C. (1997). Dynamics and thermodynamics of complex fluids. II. Illustrations of a general formalism. *Physical Review E*, 56(6), 6633. <https://doi.org/10.1103/PhysRevE.56.6633>
- [50] Nosonovsky, M., & Bhushan, B. (2009). Thermodynamics of surface degradation, self-organization, and self-healing for biomimetic surfaces. *Philosophical Transactions of The Royal Society A: Mathematical, Physical and Engineering Sciences*, 367(1893), 1607–1627. <https://doi.org/10.1098/rsta.2009.0009>
- [51] Verband der Automobilindustrie. (2010). VDA Band 2009: GPS Streulichtsensorik. Berlin: VDA. Verfügbar unter: <https://webshop.vda.de/VDA/de/vda-2009-072010>